J. Fluid Mech. (1984), *vol.* 144, *pp.* 281–295
Printed in Great Britain

Tip streaming from slender drops in a nonlinear extensional flow

By J. D. SHERWOOD
Dowell Schlumberger, B.P. 90, 42003 St Etienne, France

(Received 22 August 1983)

The deformation of inviscid and slightly viscous drops is studied using slender-body theory. The imposed axisymmetric flow is a combination of a linear extensional flow, with velocity $u_z = G_1 z$ along the axis of symmetry, together with a cubic flow $u_z = G_3 z^3$. When G_3/G_1 is sufficiently small the viscous drop breaks in a manner similar to that described by Acrivos & Lo (1978). For larger $G_3 > 0$ the drop breaks by a rapid growth at its end. Steady-state experiments in a 4-roll mill show the ejection of a column of liquid from the tip of the drop, though this is probably caused by a change in the pressure gradient rather than the mechanism described above. The ejected column then breaks into droplets via the Rayleigh instability. It is hypothesized that one or other of these mechanisms corresponds to tip streaming as observed by Taylor (1934).

1. Introduction

Recent work on the deformation of small emulsion droplets at low Reynolds numbers has concentrated on drops sufficiently small that the imposed flow is linear. When the viscosity μ_i of the drop is small compared with that of the surrounding fluid, μ, slender-body theory (Buckmaster 1972, 1973; Acrivos & Lo, 1978; Hinch & Acrivos, 1979) predicts the slender pointed drops observed by Taylor (1934), but not his observation that small drops can be ejected from the pointed ends, a phenomenon known as tip streaming. Such analyses break down close to the tip, and Sherwood (1981) suggests that the ends of the drop are actually rounded.

Here we study drops that are sufficiently large that the non-linear terms of the imposed flow must be included. The Reynolds number is assumed still to be small, and the flow $\boldsymbol{u} = (u_r, 0, u_z)$ has the form

$$u_z = G_1 z + G_3 z^3, \quad u_r = -\tfrac{1}{2}G_1 r - \tfrac{3}{2}G_3 r z^2, \quad p = 3G_3\mu(z^2 - \tfrac{1}{2}r^2),$$

where p is the pressure. Quadratic terms are excluded to maintain symmetry of the drop about $z = 0$. We have in mind the deformation of a large drop at the centre of a 4-roll mill, and in §5 we shall present some experimental results.

In a weak flow the drop is deformed only slightly away from spherical. It is straightforward to compute this deformation, but the results are of little interest to us here. Instead, we assume $\lambda = \mu_i/\mu \ll 1$. The drop becomes elongated at sufficiently high flow strengths, and we compute its shape by means of slender-body theory. We deal first in §2 with a drop of zero viscosity, and proceed in §3 to a drop which is slightly viscous. In §4 we study the evolution of drop shapes with time.

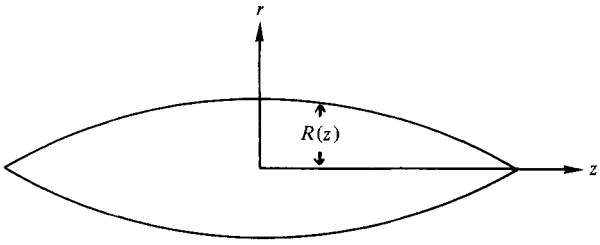

FIGURE 1. The slender drop.

2. Inviscid drop

The drop, with length l and radius $R(z)$ ($|z| \leqslant l$) is illustrated in figure 1. The imposed flow is disturbed by the presence of the drop, and this disturbance may be represented by a line distribution of sources $Q(z)$. We follow a presentation similar to that of Hinch & Acrivos (1979). The disturbance flow near the drop is a radial flow $u_r = Q/2\pi r$, with an associated stress $\sigma_{rr} = -\mu Q/\pi r^2$. Adding to this the stress due to the undisturbed flow, and substituting into the normal stress balance gives

$$p_0 - \frac{\gamma}{R} = \mu G_1 + 6\mu G_3 z^2 + \frac{\mu Q}{\pi R^2}, \tag{1}$$

where γ is the coefficient of interfacial tension between the drop and the surrounding fluid, and p_0 is the constant pressure inside the drop. Our other condition on the boundary is that the flow is tangential to the surface of the drop:

$$\frac{Q}{2\pi R} - \tfrac{1}{2}(G_1 + 3G_3 z^2) R = (G_1 z + G_3 z^3) R'.$$

Scaling all lengths by l, and scaling R by $\gamma/\mu G_1 l$, we obtain

$$(z + G_3 G_1^{-1} l^2 z^3) R' = \frac{p_0 R}{2\mu G_1} - 1 - R(1 + \tfrac{9}{2} G_3 G_1^{-1} l^2 z^2) \quad (|z| \leqslant 1), \tag{2}$$

with $R(\pm 1) = 0$. If $G_3 = 0$ this has the solution

$$R = \tfrac{1}{4}(1 - z^2),$$

where $p_0/2\mu G = P$, say, is chosen to be 3 for reasons discussed by Acrivos & Lo. If the drop has volume $\frac{4}{3}\pi a^3$, then

$$l = 20a(\mu G_1/\gamma)^2.$$

If $G_3 \neq 0$, $R(z)$ will no longer be parabolic. To ensure analyticity at $z = 0$, we look for a power-series solution of the form

$$R = a_0 + a_2 z^2 + \ldots,$$

where

$$a_0 = \frac{1}{2(P-1)}, \quad a_2 = -\frac{9 a_0 G_3 l^2}{2G_1 (3-P)}.$$

Since a_0, $-a_2 \to \frac{1}{4}$ as $G_3 \to 0$, we conclude that

$$P \sim 3 - \frac{9G_3 l^2}{2G_1} \quad \text{as} \quad \frac{G_3}{G_1} \to 0.$$

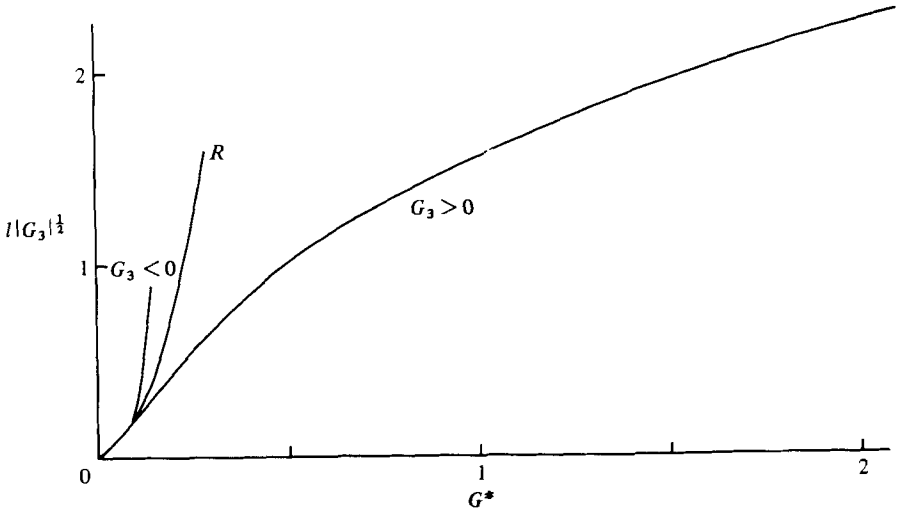

FIGURE 2. Deformation curves for an inviscid drop: non-dimensional length $l|G_3^*|^{\frac{1}{2}}$ as a function of dimensionless strain rate G^*. R would hold if the drop maintained a parabolic shape.

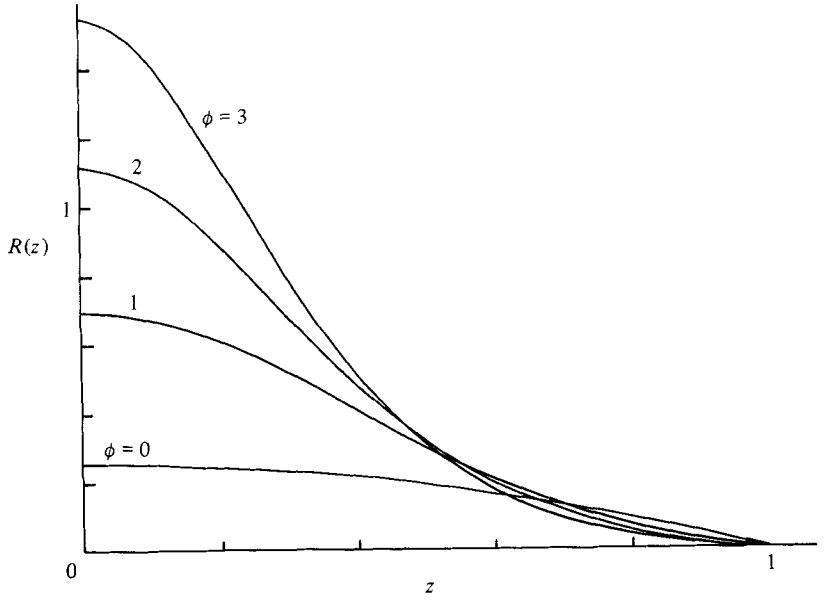

FIGURE 3. Inviscid drop shape $R(z)$ for various $\phi = G_3 l^2/G_1 > 0$.

It is straightforward to solve (2) numerically, using P as a shooting parameter to ensure that $R(1) = 0$. We obtain $R = R(z, \phi)$, where

$$\phi = G_3^* l^2, \quad G_3^* = \frac{G_3}{G_1}.$$

The volume of the drop is

$$\int_0^1 R^2 \mathrm{d}z = \frac{2a^3\mu^2 G_1^2}{3l\gamma^2},$$

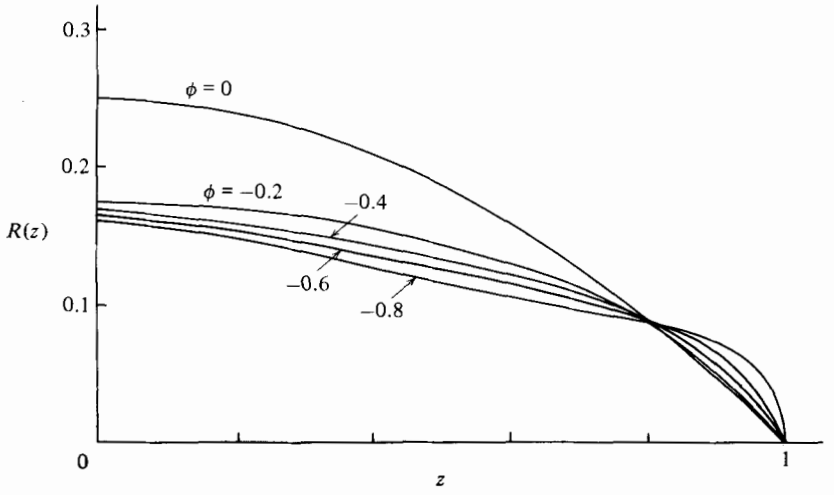

FIGURE 4. Inviscid drop shape $R(z)$ for various $\phi = G_3 l^2/G_1 < 0$.

which is a function of ϕ only. This suggests that the appropriate dimensionless rate of strain is

$$G^* = \frac{G_1 \mu a}{\gamma} (G_3^* a^2)^{\frac{1}{4}}$$

and the appropriate dimensionless drop length is $lG_3^{*\frac{1}{2}}$. In figure 2 we show $l|G_3^*|^{\frac{1}{2}}$ as a function of G^* for the two cases $G_3 \gtrless 0$, together with a comparison curve which would hold if the drop maintained a parabolic shape. We see that if G_3 is positive the drop does not grow as rapidly as it would if G_3 were zero or negative. The fluid does not wish to enter a region of high pressure. The surrounding medium is forced in this direction by viscous stresses, but no such stresses act on the drop. Solutions break down when $G_3^* l^2 = -1$, when the tip of the drop is at a stagnation point. In figures 3 and 4 we show representative drop shapes for $G_3 \gtrless 0$. Note that the vertical scale in figure 3 differs from that in all the other figures of §§2 and 3, and also that cusp-like points appear when $G_3 > 0$. In the experimental results of §5 we shall see shapes similar to those of figure 3, and we shall appeal to the above pressure arguments to explain the ejection of a fluid thread from the drop tip.

3. The viscous drop $0 < \lambda \ll 1$

We follow the same arguments as before, though we initially include time-dependence. The pressure p_{in} inside the drop is no longer uniform and a pressure gradient is established in order to ensure a return flow of fluid towards the centre of the drop:

$$\frac{R^4}{8\mu_i} \frac{\mathrm{d}p_{\text{in}}}{\mathrm{d}z} = (G_1 z + G_3 z^3) R^2 + \int_0^z 2R\dot{R} \mathrm{d}z.$$

The normal stress balance is as before (1), whilst the kinematic boundary condition becomes

$$\dot{R} + (G_1 z + G_3 z^3) R' = \frac{Q}{2\pi R} - \tfrac{1}{2}(G_1 + 3G_3 z^2) R,$$

from which we obtain

$$\dot{R}+(G_1z+G_3z^3)\,R'+R(G_1+\tfrac{3}{2}G_3z^2)+\frac{\gamma}{2\mu}-\frac{Rp_{\rm in}}{2\mu}=0,$$

where

$$p_{\rm in}=p_0+8\mu_{\rm i}\int_0^z\left\{(G_1z+G_3z^3)\,R^{-2}+R^{-4}\int_0^z 2R\dot{R}\,{\rm d}z\right\}{\rm d}z.$$

Differentiating with respect to z puts the governing equation in the form

$$(G_1z+G_3z^3)\,(RR''-R'^2)+(G_1+3G_3z^2)\,RR'+9G_3zR^2+\dot{R}_z\,R$$
$$-\dot{R}R'-\frac{\gamma R'}{2\mu}=4\lambda\left(G_1z+G_3z^3+2R^{-2}\int_0^z R\dot{R}\,{\rm d}z\right).$$

Note that the inclusion of cubic terms has not substantially modified the governing equation found by Acrivos & Lo. Scaling all lengths by l, then scaling R by $\gamma/G_1\mu l$ and dropping time dependence we obtain

$$(z+G_3^*l^{*2}z^3)\,(RR''-R'^2)+RR'(1+3G_3^*l^{*2}z^2)+9G_3^*l^{*2}zR^2-\tfrac{1}{2}R'$$
$$=4\Gamma^2(z+G_3^*l^{*2}z^3),\qquad(3)$$

with $R(\pm1)=0$, where $l^*=l\lambda^{\frac{1}{3}}/a$ and $G^*=G_1\mu a\lambda^{\frac{1}{6}}/\gamma$ are the non-dimensional length and flow strength used by Acrivos & Lo, $G_3^*=G_3a^2/G_1\lambda^{\frac{2}{3}}$ and $\Gamma=G^*l^*=$ Acrivos & Lo's K^{-1}. G_3^* depends on the form of the flow, G_3/G_1, but not on its absolute magnitude, which varies with G^*. It is therefore appropriate to watch the deformation of an individual drop by varying G^* whilst holding G_3^* constant.

When $G_3=0$ there is an analytic solution

$$R(z)=\alpha(1-z^2),\qquad(4)$$

where

$$\alpha=\tfrac{1}{8}(1\pm(1-64\Gamma^2)^{\frac{1}{2}}),\qquad(5)$$

and on integrating to find the volume of the drop, we obtain

$$G^*=\frac{(\frac{1}{20}l^*)^{\frac{1}{2}}}{1+\frac{4}{5}l^3}.$$

When $G_3\neq0$ we must solve (3) numerically. We first examine the solution near $z=1$. Expanding as a power series in $s=1-z$, we look for a solution of the form

$$R=a_1s+a_2s^2+bs^\beta+\ldots,\qquad(7)$$

where

$$a_1=\frac{1\pm(1-64\Gamma^2(1+G_3^*l^{*2})^2)^{\frac{1}{2}}}{4(1+G_3^*l^{*2})},\qquad(8)$$

and from linear theory we know that we should take the + sign when G^* is small. Thus

$$a_1<\tfrac{1}{2}(1+G_3^*l^{*2})$$

and

$$\beta=3-\frac{1}{2a_1(1+G_3^*l^{*2})}<2,$$

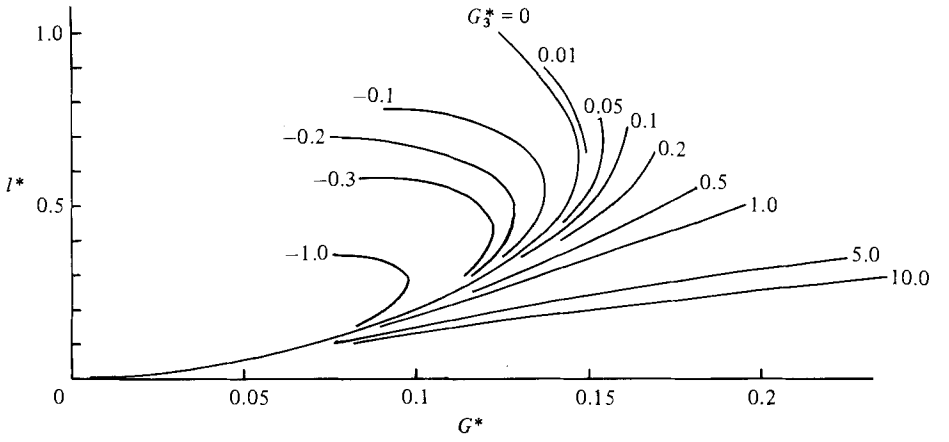

FIGURE 5. Deformation curves for viscous drops, presented in the same manner as Acrivos & Lo (1978). Dimensionless length $l^* = l\lambda^{\frac{1}{3}}/a$ as a function of the flow strength $G^* = G_1\mu a\lambda^{\frac{1}{3}}\gamma^{-1}$, for various nonlinear flows $G_3^* = G_3a^2/G_1\lambda^{\frac{2}{3}}$.

but b is not determined by the expansion. At $O(s)$ we obtain

$$a_2 = -\frac{4\Gamma^2(1+3G_3^*l^{*2})}{1-2a_1(1+G_3l^{*2})}.$$

The numerical scheme was as follows. First l^* was chosen (with l^* initially close to zero, so that $G_3^*l^{*2}$ was small and the drop shape close to that for a linear flow). G^* and b were then guessed and the expansion (7) was used to give R close to the tip $z = 1$. A fourth order Runge–Kutta method was used to integrate the differential equation back towards the origin, stopping short to avoid the singularity there. The solution was then extrapolated into $z = 0$. $R'(0)$ should be zero, and the volume of the drop should satisfy

$$\tfrac{2}{3}G^{*2}/l = \int_0^1 R^2\mathrm{d}z.$$

G^* and b were varied until these two conditions were satisfied. l^* was then increased and the process repeated. In figure 5 we show the resulting deformation curves. When $G_3^* = 0$ the drop length grows as the flow strength increases, until $G^* = 0.148$ and $l^* = 0.63$. There are no steady solutions for higher values of G^*, and the drop grows ever longer, maintaining a parabolic shape (Buckmaster 1973). This is in agreement with the analytic deformation curve (6). The curve continues to higher values of l^*. Acrivos & Lo showed that the lower portion of the curve is stable to infinitesimal disturbances and the upper portion unstable. $G^* = 0.148$ corresponds to a point of neutral stability. The numerical scheme was satisfactory as long as

$$1-64\Gamma^2(1+G_3^*l^{*2})^2 > 0, \tag{9}$$

so that the square root in the expansion near the tip (8) is real. When $G_3^* = 0$ a second branch of (unstable) solutions exists, corresponding to the choice of the negative sign in (5). This could not be found numerically since $\beta < 1$ and the expansion of $R(s)$ for small s breaks down. Numerical breakdown occurred when $l^* = 1.0$, $G^* = 0.125$. Analytically, breakdown should have occurred when $l^* = 1.12$ and $G^* = 0.112$. Thus our numerical length is too small by 12%, giving an idea of the accuracy achieved at the extreme points of the curves. In figure 6 we show drop shapes when $G_3^* = 0$ for comparison with later results for shapes in nonlinear flows.

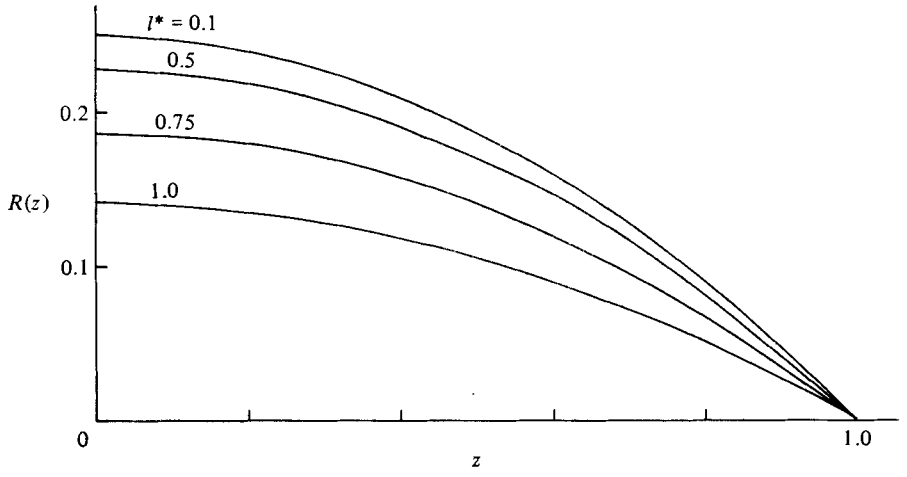

FIGURE 6. Viscous drop shapes in a linear flow, $G_3^* = 0$, as given by (4).

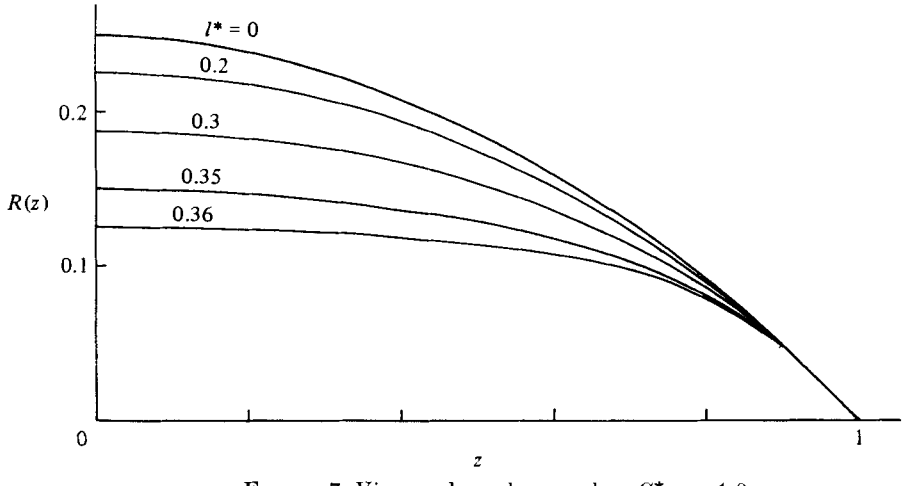

FIGURE 7. Viscous drop shapes when $G_3^* = -1.0$.

The deformation curves for $G_3^* < 0$ are similar to those for a linear flow: the mechanism of break-up is basically the same and is discussed in §4. As in the inviscid case, the drop length grows more rapidly than when $G_3 = 0$. Typical drop shapes are shown in figure 7.

When $G_3 > 0$ the drop length grows more slowly. Drop shapes are shown in figure 8. The drops become more pointed as G_3^* increases, but from the expansion (6) near $z = 1$ we see that cusps never develop. If $G_3^* < 0.1$ the deformation curve turns back on itself, and break-up occurs as for the linear flow. If $G_3^* > 0.1$ we find that (9) is violated before the curve turns. There are no steady-state solutions for higher flow strengths, and the mechanism of drop break-up is different. It is difficult to study this breakdown of the solution, as only a numerical solution is available to us. Some insight can be gained by re-examining time-dependent stability in the case $G_3 = 0$. Suppose the drop shape has the form

$$R = \alpha(1 - z^2 + \delta g(z)\, e^{\sigma t})$$

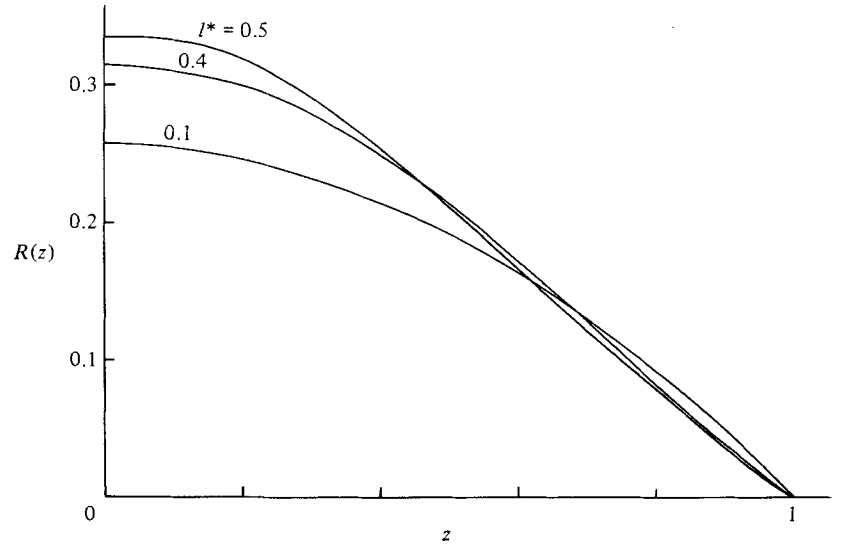

FIGURE 8. Viscous drop shapes when $G_3^* = 1.0$.

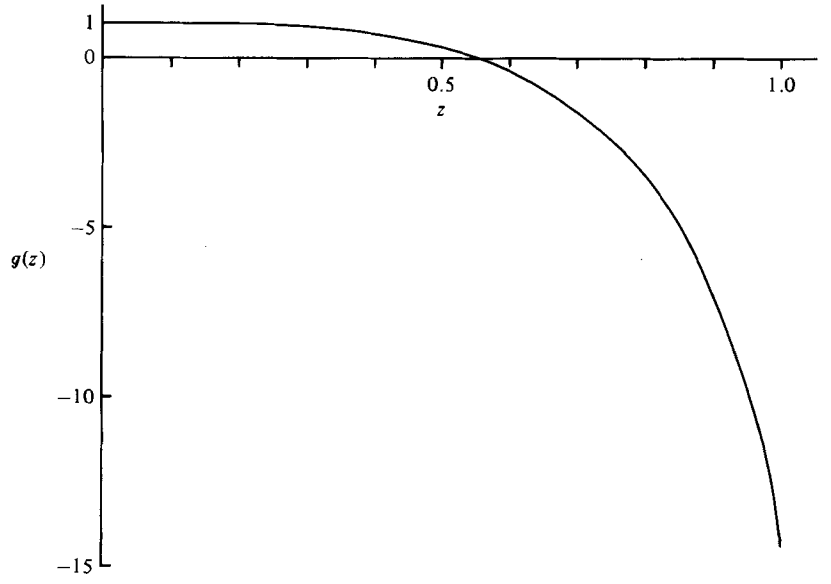

FIGURE 9. Marginally stable volume-preserving perturbation (11) with rapid growth at the drop tip, corresponding to the case $64\Gamma^2 = 1$ in (5).

for some small δ. In the marginally stable case $\sigma = 0$, g satisfies

$$g''(z-z^3)+g'(3z^2+1+\tfrac{1}{2}\alpha^{-1})-4zg = 0,$$

with solutions

$$g_1(z) = 1-z^2/s_1^2,$$

$$g_2(z) = g_1(z)\int_1^z (1-s^2)^{2-\frac{1}{4}\alpha^{-1}} s^{\frac{1}{2}\alpha^{-1}-1}\left(1-\frac{s^2}{s_1^2}\right)^{-2} \mathrm{d}s,$$

where $s_1^2 = \frac{1}{4}\alpha^{-1} - 1$. In general we reject g_2 to maintain analyticity at $z = 0$. A volume-preserving solution must satisfy

$$\int_0^1 R(z)\, g(z)\, \mathrm{d}z = 0. \tag{10}$$

Hence, when $G_3 = 0$, instability occurs at $\alpha = \frac{5}{24}$, when

$$g = 1 - 5z^2.$$

This corresponds to Buckmaster's shape-preserving solution and to $G^* = 0.148$. However, if $\alpha = \frac{1}{8}$ (corresponding to violation of (9)), we can evaluate the integral for g and obtain

$$g = B((1-z^2)\log(1-z^2)+1)+(1-B)(1-z^2). \tag{11}$$

This is analytic at $z = 0$ and has an adjustable parameter B. It is straightforward to show that $B = -14.36$ is volume-preserving (10). In figure 9 we show this perturbation. There is a very rapid growth at the end of the drop, together with a slight decrease in the radius of the rest of the drop. This type of break-up is not usually observed when $G_3 = 0$ because the shape-preserving instability occurs first. Our numerical calculations show that tip growth will occur if $G_3^* > 0.1$.

We cannot easily find g when $G_3 \neq 0$, as we have no analytic expression for R, but the degree of freedom represented by B will ensure that there is a volume-preserving perturbation. The numerical calculations predict that $G_3^* l^{*2}$ is still small at break-up. An attempt to use this as a small perturbation parameter went singular as α approached $\frac{1}{8}$.

4. Time-dependent studies

The above arguments, while plausible, are still somewhat vague, and in order to confirm them a time-dependent numerical study was performed. Following Acrivos & Lo we non-dimensionalize time by $1/G_1$, lengths in the radial direction by $a\lambda^{\frac{1}{6}}$, lengths in the axial direction by $a\lambda^{-\frac{1}{3}}$ and pressures by $2\mu G_1$. As before we take $G^* = G_1\mu a\lambda^{\frac{1}{6}}/\gamma$, $G_3^* = G_3 a^2/G_1\lambda^{\frac{2}{3}}$. The governing equations become

$$p_{\mathrm{in}} = p_0 + 4\int\left\{(z+G_3 z^3)R^{-2} + 2R^{-4}\int_0^z R\dot{R}\,\mathrm{d}z\right\}\mathrm{d}z,$$

$$\dot{R} + R'(z+G_3^* z^3) + (1+\tfrac{9}{2}G_3^* z^2)R + \tfrac{1}{2}/G_1^* - p_{\mathrm{in}} R = 0.$$

The numerical scheme was taken directly from Hinch & Acrivos (1980). We represent R by the expansion

$$R(z,t) = R_0(t) + R_1(t)\, z^2 + \ldots + R_N(t)\, z^{2N}.$$

This is substituted into the governing equations. $\dot{R}_n$ is obtained by comparing coefficients of powers of z. The program therefore has to be able to multiply and divide two polynomials. $\dot{R}$ is evaluated for two arbitrary values of p_0, and then, making use of the linearity of R in p_0, we choose that linear combination of the solutions which preserves the volume of the drop by ensuring

$$\int_0^l R\dot{R}\,\mathrm{d}z = 0.$$

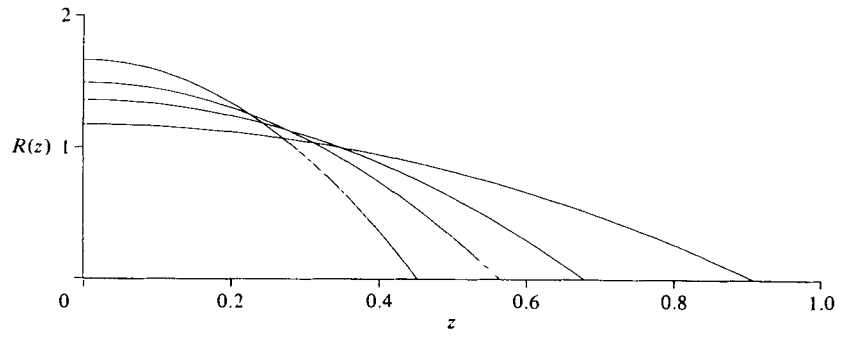

FIGURE 10. Unstable drop growth when $G_3 = 0$. The flow strength is increased from $G^* = 0.14$ to $G^* = 0.16$ at time $t = 0$. One quadrant of the drop shape is shown at $t = 0$, 2, 4 and 6.

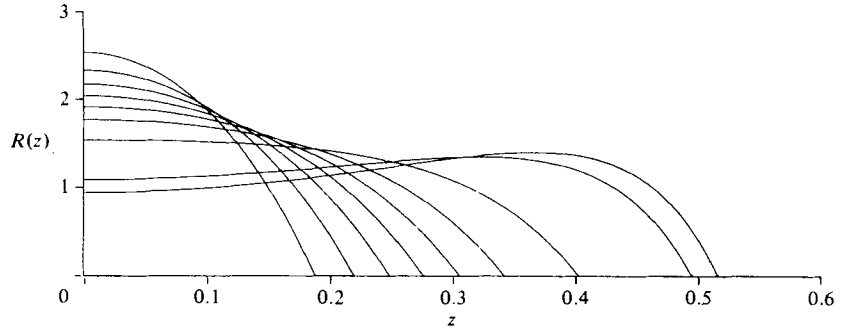

FIGURE 11. Unstable drop growth when $G_3^* = -1.0$. The flow strength is increased from $G^* = 0.09$ to 0.11 at time $t = 0$. The drop shape is shown at $t = 0$, 1, 2, 3, 4, 5, 6, 6.7 and 6.8.

While provision was made to correct any slow drift in the drop volume, this correction was never required except at the first time step if the initial drop shape was not specified with sufficient accuracy.

The program was checked against the analytic solution available for $G_3 = 0$. For $N = 11$ break-up occurred when G^* was between 0.147 and 0.148. The equilibrium length at $G^* = 0.14$ agreed with the analytic result to 3 significant figures. Results were identical for other values of N, and this reminds us that for this case $N = 1$ would suffice. In figure 10 we watch the evolution of the drop shape with time t. At $t = 0$ the drop has the equilibrium shape corresponding to $G^* = 0.14$. The flow rate G^* is increased to 0.16 and the shape $R(z)$ is plotted at times $t = 0, 2, 4$ and 6. The step length was $\Delta t = 0.05$. Halving this length gave identical results. The drop maintains its parabolic shape.

When $G_3^* = -1$ results for equilibrium drop lengths with $N = 7$ and with $N = 13$ were identical. Increasing N to 13 did not change the values of R_0 up to R_7. Break-up is predicted between $G^* = 0.96$ and 0.97, which may be compared with the value 0.98 obtained in §3. In figure 11 we watch the evolution of a drop that is initially in equilibrium at $G^* = 0.09$. At time zero the flow strength is increased to 0.11, and drop shapes are shown at subsequent times. The computations eventually broke down because of numerical overflow. The drop length is increasing gradually, and it appears that the drop will snap at the centre.

More difficulty was encountered for the case $G_3^* = +1$. Low values of N showed

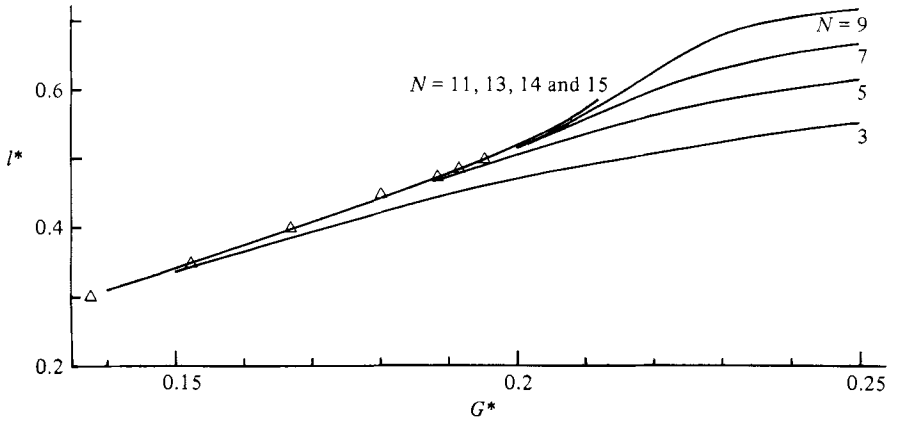

FIGURE 12. Deformation curves for stable drop lengths as given by the time-dependent scheme of §5. △, points obtained by the finite-difference scheme of §3 (c.f. figure 5). $G_3^* = 1.0$.

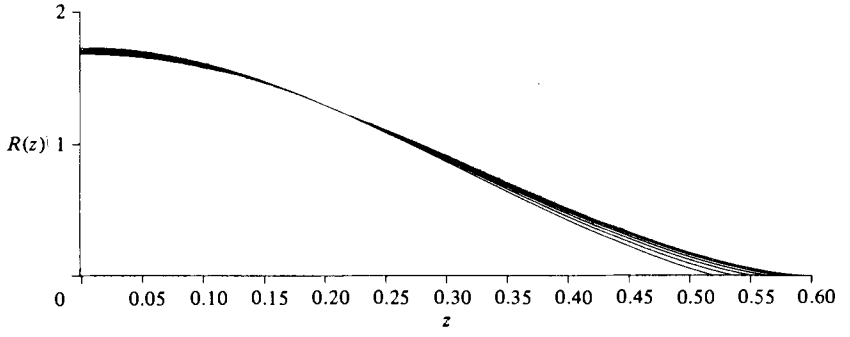

FIGURE 13. Unstable drop growth when $G_3^* = 1.0$. The flow strength is increased from $G^* = 0.21$ to 0.23 at time $t = 0$. The drop shape is shown at $t = 0$, 0.2, 0.4, 0.6, 0.8 and 1.0.

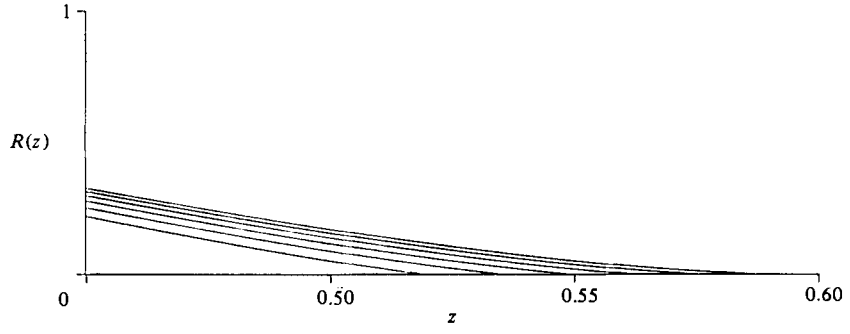

FIGURE 14. Unstable drop growth when $G_3^* = 1.0$. Detail of tip growth from figure 13.

no unusual behaviour at the point where break-up was expected. Results are shown in figure 12. Those for $N = 11$, 13 and 14 are identical with those for $N = 15$. Also shown are the calculations of §3, which are in good agreement but which end at $G^* = 0.19$ rather than the 0.212 found in this section. In §3 we showed that the results did not reach all the way to the singularity (for the case $G_3 = 0$). On the other hand, the end of the drop is the place where the expansions of this section are most likely to break down.

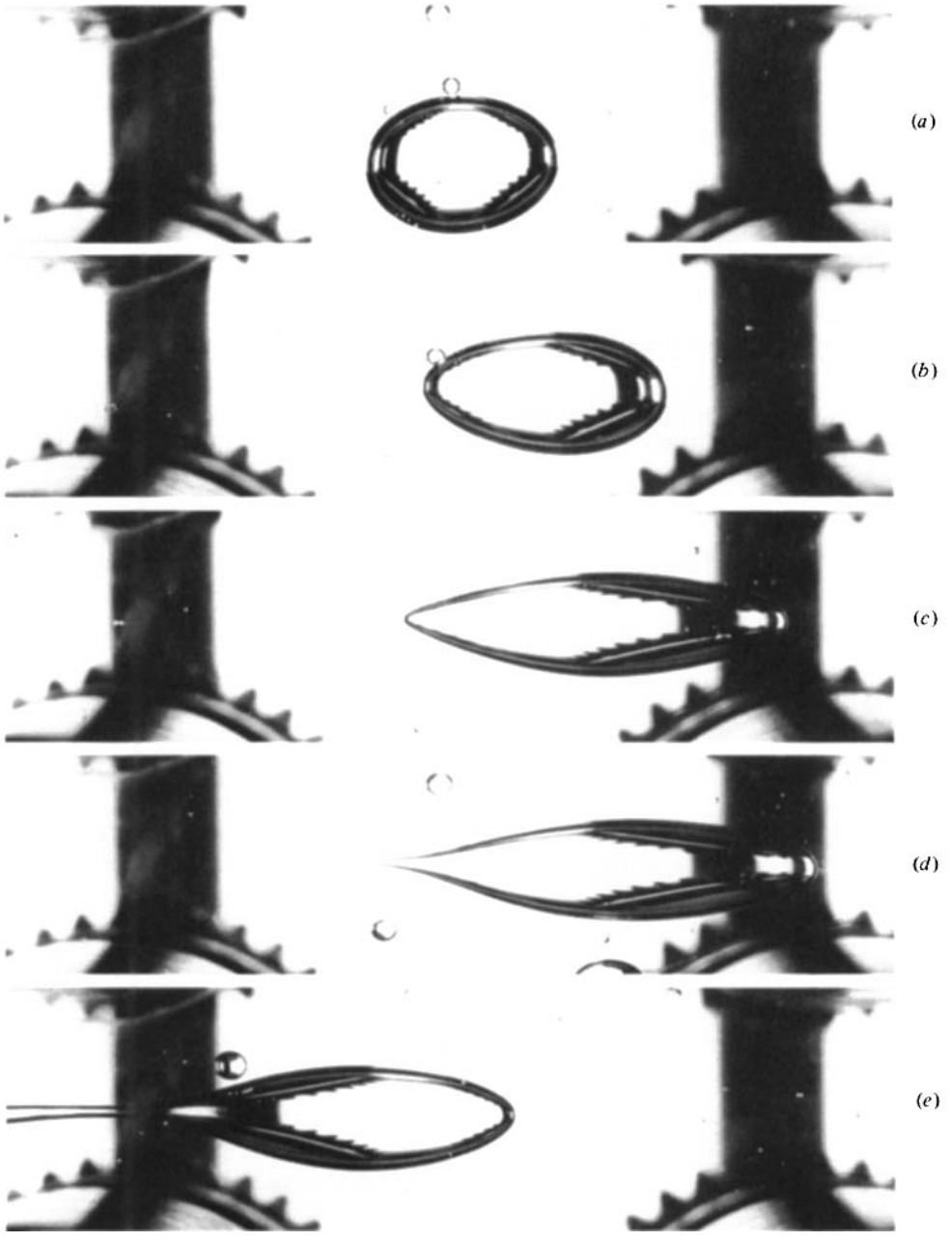

FIGURE 15. Drop of water surrounded by castor oil, at the centre of the 4-roll mill, at increasing flow strengths.

In figure 13 we watch evolution of a drop when $G_3^* = +1$. The drop starts in equilibrium at $G^* = 0.21$, and the flow strength is increased to $G^* = 0.23$ at time zero. Only the tip of the drop is being pulled out, and a cusp develops. The length of the drop is found numerically by solving $R(l) = 0$. The root becomes a double root, and vanishes. Figure 14 is an enlargement of the relevant portion of figure 13. Just as in §3, we find that the drop breaks owing to rapid growth solely at its tip.

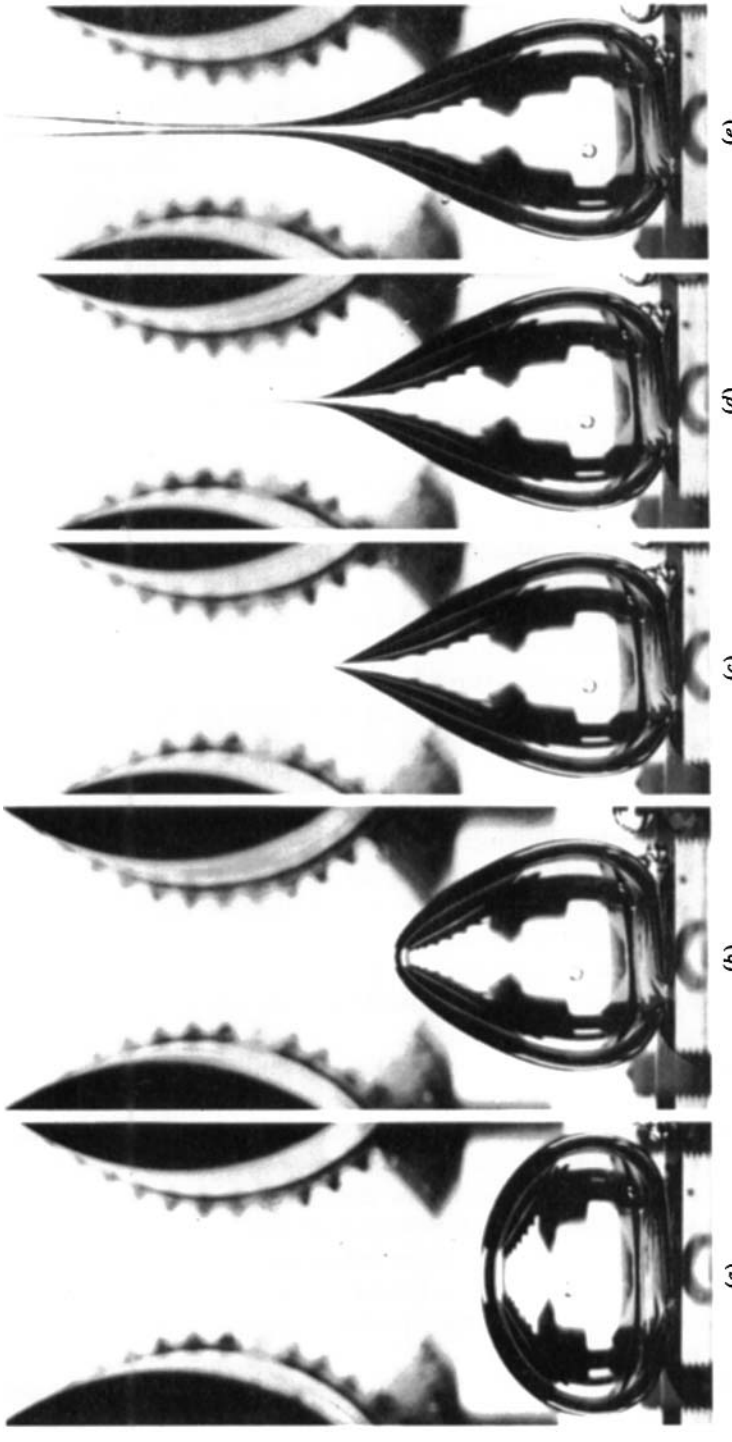

FIGURE 16. Water drop at the bottom of the mill, at increasing flow strengths.

5. Experiments

A few simple observations of drop shape were made in a 4-roll mill with dimensions similar to those of Taylor's (1934) mill. The rolls of diameter 24 mm were on axes 32 mm apart in a perspex box with dimensions $75 \times 75 \times 38$ mm, and the centres of the lower rolls were 22 mm above the base of the box. The speeds of the left and right pairs of rolls could be varied independently, but were not calibrated. Our results are therefore only qualitative. Because the maximum speed of the rolls was low, it was possible to break only large drops, of a size comparable with the gap in the 4-roll mill. The photographs show water drops in castor oil, for which the viscosity ratio λ is 1.2×10^3.

In figure 15 we show a drop at the centre of the apparatus. A pointed end develops in figure 15(*d*). In figure 15(*e*) (which is the same drop, but which was not taken immediately after figure 15(*d*)) we see the ejection of a column of water. This eventually breaks via the Rayleigh instability into a series of small droplets, though not usually until after it has passed through the nip.

Because the density of castor oil is about 960 kg m^{-3}, the water drop will sink to the bottom of the mill when the rolls are stationary. Surface tension is not sufficiently strong to keep a large drop spherical (figure 16*a*). The drop can then be deformed, using gravity to keep it stationary. The deformation point at increasing flow strengths is shown in figures 16(*b–e*). A point has developed in figure 16(*c*). The stationary tip can be observed through a travelling microscope, and appears to have a finite radius. In figure 16(*d*) a thread is ejected from the drop tip. The thread is thin and uniform, and consequently breaks into drops of uniform size. Because the volume of the main drop decreases very slowly the process is steady and observations can be made until recirculating drops obscure the field of view. The entire system of drop and column appears cylindrically symmetric, though the tip of the drop is obscured by the rolls when looking from the side. If the roll speed is increased the column diameter grows and the resulting drops are larger (figure 16*e*). Decreasing the speed reduces the diameter, though at a critical speed the column breaks off and disappears, rather than becoming infinitesimally thin.

The photographs show a fresh drop. If left overnight a skin develops. Switching on the rolls forces the skin to the tip of the drop, from where it is pulled off, exposing a clean interface.

The extension rate along the centreline of a 4-roll mill has been measured by Fuller *et al.* (1980). Their roll configuration is nearly a scaled form of that used here, though their surrounding walls are further away. The extension rate increases away from the centre of the mill and the break-up mechanism discussed in §§3 and 4 could operate here. The drop in figure 16(*c*) resembles those of figures 3 and 8. However, the mechanism of break-up observed in figure 16 is probably not that found numerically. It is hard, because of parallax, to tell just where our drop breaks, but it is close to the point of maximum extension rate found by Fuller *et al.* The pressure gradient becomes negative at this point, and the tip of the drop will flow rapidly into the region of low pressure, as discussed in §2.

Taylor's (1934) tip streaming (the ejection of a series of individual drops) was never observed in these experiments with either water or silicone-oil drops. We cannot tell whether to associate it with the numerically predicted mechanisms of §§3 and 4, or with the two-stage process of ejection of a liquid column, followed by Rayleigh break-up, observed experimentally in §5.

I am grateful to Dr E. J. Hinch of Cambridge for helpful correspondence and for suggesting the analysis of §4; and to Mr M. Titley, of Unilever Research, Port Sunlight, for photography.

REFERENCES

ACRIVOS, A. & LO, T. S. 1978 Deformation and breakup of a single slender drop in an extensional flow. *J. Fluid Mech.* **86**, 641.

BUCKMASTER, J. 1972 Pointed bubbles in slow viscous flow. *J. Fluid Mech.* **55**, 385.

BUCKMASTER, J. 1973 The bursting of pointed drops in slow viscous flow. *Trans. ASME* E: *J. Appl. Mech.* **40**, 18.

FULLER, G. G., RALLISON, J. M., SCHMIDT, R. L. & LEAL, L. G. 1980 The measurement of velocity gradients in laminar flow by homodyne light-scattering spectroscopy. *J. Fluid Mech.* **100**, 555.

HINCH, E. J. & ACRIVOS, A. 1979 Steady long slender droplets in two-dimensional straining motion. *J. Fluid Mech.* **91**, 401.

HINCH, E. J. & ACRIVOS, A. 1980 Long slender drops in a simple shear flow. *J. Fluid Mech.* **98**, 305.

SHERWOOD, J. D. 1981 Spindle-shaped drops in a viscous extensional flow. *Math. Proc. Camb. Phil. Soc.* **90**, 529.

TAYLOR, G. I. 1934 The formation of emulsions in definable fields of flow. *Proc. R. Soc. Lond.* A**146**, 501.